Institute of Paper Science and Technology
Atlanta, Georgia

IPST Technical Paper Series Number 778

The Effect of Fiber Consistency on Bubble Size

T.J. Heindel and A.E. Garner

April 1999

Submitted to
Nordic Pulp and Paper Research Journal

INSTITUTE OF PAPER SCIENCE AND TECHNOLOGY
PURPOSE AND MISSIONS

The Institute of Paper Science and Technology is an independent graduate school, research organization, and information center for science and technology mainly concerned with manufacture and uses of pulp, paper, paperboard, and other forest products and byproducts. Established in 1929, the Institute provides research and information services to the wood, fiber, and allied industries in a unique partnership between education and business. The Institute is supported by 52 North American companies. The purpose of the Institute is fulfilled through four missions, which are:

- to provide a multidisciplinary education to students who advance the science and technology of the industry and who rise into leadership positions within the industry;
- to conduct and foster research that creates knowledge to satisfy the technological needs of the industry;
- to serve as a key global resource for the acquisition, assessment, and dissemination of industry information, providing critically important information to decision-makers at all levels of the industry; and
- to aggressively seek out technological opportunities and facilitate the transfer and implementation of those technologies in collaboration with industry partners.

ACCREDITATION

The Institute of Paper Science and Technology is accredited by the Commission on Colleges of the Southern Association of Colleges and Schools to award the Master of Science and Doctor of Philosophy degrees.

NOTICE AND DISCLAIMER

The Institute of Paper Science and Technology (IPST) has provided a high standard of professional service and has put forth its best efforts within the time and funds available for this project. The information and conclusions are advisory and are intended only for internal use by any company who may receive this report. Each company must decide for itself the best approach to solving any problems it may have and how, or whether, this reported information should be considered in its approach.

IPST does not recommend particular products, procedures, materials, or service. These are included only in the interest of completeness within a laboratory context and budgetary constraint. Actual products, procedures, materials, and services used may differ and are peculiar to the operations of each company.

In no event shall IPST or its employees and agents have any obligation or liability for damages including, but not limited to, consequential damages arising out of or in connection with any company's use of or inability to use the reported information. IPST provides no warranty or guaranty of results.

The Effect of Fiber Consistency on Bubble Size

Theodore J. Heindel and Adele E. Garner, Institute of Paper Science and Technology

Keywords: Bubble size distribution, Flash x-ray radiography, Flow visualization, Gas flows, Pulp suspensions

SUMMARY

Bubble size control is very important whenever a gas is introduced into a liquid. However, in the pulp and paper industry, bubble size is difficult to measure due to the presence of fibers. This study used flash x-ray radiography (FXR), an x-ray process that provides stop-motion images, to visualize gas bubbles in fiber suspensions. FXR images of air bubbling through northern bleached softwood kraft pulp suspensions at consistencies from 0 to 1.5% were taken, and bubble size distributions were determined for a fixed gas flow rate.

The presence of fibers promoted large bubble formation, which created churn-turbulent flow conditions. These bubbles also acted as "mobile mixers" and maintained a well-mixed system. The remaining small bubbles, defined as those with effective bubble diameters $d \leq 12$ mm, were characterized by various distribution functions. It was shown that a single lognormal distribution was adequate to predict the bubble size distribution when $d \leq 12$ mm for all consistencies addressed in this study.

ADDRESS OF THE AUTHORS
500 10th Street, NW
Atlanta, GA 30318-5794
USA

INTRODUCTION

Bubble size is very important to many processes in the pulp and paper industry. During bleaching with gaseous chemicals, such as oxygen or ozone, the gas bubbles should be small, uniform in size, and homogeneously distributed throughout the system to maximize the mass transfer surface area and ensure bleaching uniformity. A homogeneous bubble size distribution is also important in direct contact steam heating applications. In this process, small steam bubbles are preferred to maximize the heat transfer surface area and eliminate channeling. In contrast, for gas removal from fiber suspensions, bubble coalescence should be encouraged to form large bubbles, thereby creating a corresponding large buoyant force, encouraging bubble removal. Finally, in flotation deinking, a bubble size distribution of relatively small bubbles is preferred to provide a range of bubble sizes with which various contaminant sizes can interact to form bubble/particle aggregates.

The gas/liquid/fiber flows described above are complex slurry flows because the fibers have a density close to that of water and can form flocs at consistencies as low as 0.3% by weight, and continuous fiber networks at consistencies greater than 1% (Kerekes et al. 1985). When a gas is introduced into the fiber suspension, fiber network formation and flocculation can trap bubbles, preventing their rise to the surface. Individual bubbles must either bypass the flocs or coalesce with other bubbles to form a resultant bubble with a sufficient buoyant force to break through the network (Pelton, Piette 1992). If the fiber consistency is too high, preferential bubble rise paths may form in a fiber suspension where locally high fiber consistency regions (i.e., high floc concentration) prevent bubble ascension, and most bubbles are diverted to rise in locally low consistency regions. This process is typically referred to as channeling and is detrimental to any process where homogeneous flow conditions are required for optimal performance.

A severe impediment to effective bubble size control in a pulp suspension is the difficulty in measuring it at typical operating consistencies. Bubble size can be easily measured in a transparent (i.e., gas/water) system by optical visualization and/or laser techniques (Clift et al. 1978; Hetsroni 1982; Saxena et al. 1988; Zhu 1996). If the system is opaque, optical and laser techniques can only be utilized near the system boundaries, if at all. However, the walls encompassing the system can influence the information obtained and it may not represent true conditions in the bulk flow. For these systems, resistivity or optical probes have been suggested, but they would be inadequate in a fiber suspension because fibers could form entanglements around the probe tip.

Initial attempts to visualize gas/liquid/fiber suspensions have been conducted by Walmsley (1992). When as little as 0.1% by weight of fiber was added to water, a significant change in the bubble behavior was observed. Water was also replaced by clove oil to produce a system with the same refractive index as cellulose fiber to allow for bubble visualization at higher consistencies. Observations revealed that the fibers inhibited upward bubble motion and channels of low fiber concentration formed where the majority of bubbles rose. Hunold et al. (1997) measured bubble size in dilute fiber systems of less than 0.5% consistency by suctioning a small sample out of the test cell and passing it through a capillary tube. Intermittent gas volumes were recorded and translated to equivalent gas bubble diameters, assuming no bubble coalescence occurred in the capillary tube or suction head, which is a good assumption if the bubble is small and coated with a surfactant. Bubble size in fiber suspensions has also been obtained by Ajersch et al. (1992) by isolating samples in a transparent flow cell. When the flow was stopped, the bubbles were allowed to rise to the surface for photographic analysis. This procedure also assumed negligible bubble coalescence and all bubbles present were free to rise to

the surface. Bubble size measurements have also been obtained in air/water systems to calibrate air injectors used in flotation deinking studies (Julien Saint Amand 1997). This information was then utilized to relate bubble size to flotation deinking performance, although the calibration was performed in the absence of fibers. However, the presence of fibers may have a significant effect on bubble coalescence and size, so actual bubble size during the flotation experiments may have changed considerably.

Radiation techniques have recently been used to quantify bubble flow characteristics in gas/liquid/fiber systems. Lindsay et al. (1995) and Schulz and Heindel (1998) utilized γ-ray densitometry to measure chord average gas holdup (defined as the average gas percent by volume along the chord joining the γ-ray emitter and detector) in air/water/cellulose fiber systems. This technique involved recording, via a detector, the γ-rays emitted from a γ-source and transmitted through an object or region of interest over a period of time. However, local bubble characteristics (e.g., bubble size) were not obtained with this particular radiation technique. One radiation technique that can be used to visualize gas bubble size and flow structures in a gas/liquid/fiber system involves x-rays, called flash x-ray radiography (FXR). This is a process where an intense burst of x-rays is produced for a fraction of a second to record dynamic events on film that cannot be captured by conventional photography. Recently, FXR has been used to observe gas flow patterns (Heindel, Monefeldt 1997, 1998) and measure bubble size (Heindel 1999) in old newspaper suspensions at consistencies as high as 1.5% and 1.0%, respectively. This is the range typical of flotation deinking.

In this study, FXR has been used to determine bubble size distributions in a quiescent (no bulk fluid movement) bubble column filled with northern bleached softwood kraft (NBSK) pulp suspensions at consistencies of up to 1.5%.

EXPERIMENTAL PROCEDURES

A schematic representation of the experimental setup used in this study is shown in *Fig. 1*. The x-ray unit was a 300 keV HP 43733A flash x-ray system (currently supported by Maxwell Physics International, San Leandro, CA, USA), which generated a 30 nanosecond x-ray pulse. The fast x-ray pulse provided stop-motion x-rays of air, injected at the column base, moving through the pulp suspension. A single 20 cm × 25.2 cm x-ray negative was exposed during each discharge of the x-ray unit. Qualitative observations of the general gas flow patterns were obtained in the bubble column by taking separate x-rays at one of four column positions. Complete details of the FXR procedures can be found in Heindel and Monefeldt (1998).

The bubble column was 1 m tall with a rectangular cross section of 20 cm × 2 cm, and was constructed with face panes of 6.35 mm clear acrylic stock. Compressed and filtered air was injected into the base of the column through a sintered bronze sparger with a nominal pore size of 40 μm. This was attached to the end of a flexible air line and placed on the bottom of the column. The air line was positioned near the column wall such that it did not interrupt the bulk bubble flow patterns. An air flow rate of 2 lpm (liters per minute) was fixed with a Dixon air regulator and filter for all experiments, and was measured with a Sierra Instruments mass flow meter. This air flow rate corresponded to a superficial gas velocity (volumetric gas flow rate divided by the column cross-sectional area) of 0.83 cm/s. The entire bubble column was mounted on a support stand with locking wheels to allow horizontal placement from the x-ray source.

The bubble column was charged by filling it from the top with 3.2 L of the desired water/fiber slurry and corresponded to a column fluid height of 80 cm. This allowed for fluid expansion in the column once air was introduced into the system. The column was drained when

not in use through a valved opening located on the column side near its base. The air flow rate of 2 lpm was sufficient to keep the fiber suspension well mixed during the image acquisition.

The system of interest was composed of deionized water with or without NBSK pulp, through which filtered air was bubbled. The NBSK dry lap pulp was reslushed following TAPPI Method T 205 om-88 (1994); however, deionized water was used, and disintegration was performed at 1.2-1.3% consistency. Pulp slurries of 0.1, 0.5, and 1.0% consistency were prepared by diluting samples of the reslushed stock with deionized water. Slurries with consistencies greater than 1.2% were prepared by filtering water from the reslushed stock until the desired consistency was obtained (i.e., 1.5%). A representative fiber sample was analyzed to determine a 2.8 mm weight-weighted fiber length (Kajaani FS-100 fiber length analyzer) and a 0.3% ash content (TAPPI Method T413 om-93 (1996)).

Once the FXR images acquired in this study were developed, they were analyzed using Optimas image analysis software. The image analysis pixel size in this study was 0.14 mm/pixel and bubbles larger than 1 mm in diameter were recorded for analysis. Bubble size measurements were obtained from multiple x-rays taken at column position 2. Bubble areas were recorded and converted to equivalent bubble diameters, defined as the diameter of the circle whose area was equal to that of the bubble image.

RESULTS

Flash x-ray radiographs were obtained at four positions in a quiescent bubble column filled with various consistencies of NBSK pulp. General air flow patterns will first be described and then bubble size measurements at column position 2 will be presented.

The composite of four x-ray images for an air/water system (0% consistency) is presented in *Fig. 2*. This provides a baseline for all other comparisons. Each image was taken at a separate

time interval and the gaps between images are the result of fixed, non-overlapping regions where the x-ray film cassette was located. Although the x-ray film was 20 cm × 25.2 cm, the area of each x-ray image shown in *Fig. 2* is 20 cm × 20 cm. The remaining film area extended beyond the column sides and contained image and location identifiers, which were digitally removed for clarity in the figures presented here. The flexible tubing used to supply the air is clearly visible on the left-hand side of the column. The general flow patterns in the bubble column are captured in *Fig. 2*. Many small bubbles are observed throughout the column (the small dark regions in each radiograph) and this flow regime is generally termed bubbly (Hewitt 1982). The bubbles are relatively small, rise in a turbulent fashion, and encompass the entire column width. Backmixing is also visually observed and results in the many small bubbles recorded on the left-hand side of position 1 in *Fig. 2*. The gas holdup of the system is visible as shown by the rise in the air/fluid interface from the initial column height of 80 cm to approximately 84 cm. This corresponds to an approximate gas holdup of 5%.

The flow patterns observed in *Fig. 2* differ slightly from those observed by Heindel and Monefeldt (1997, 1998) and Heindel (1999) because the air injection method and air flow rate are different. Heindel and Monefeldt (1997, 1998) used a septum with nine evenly spaced holes to introduce air into the same column as that used here, and covered a wide range of air flow rates from 0.25 to 30 lpm. In contrast, Heindel (1999) used either a septum with a single hole or a sparger to introduce air into the same column, but the air flow rate was fixed at 0.25 lpm.

Adding as little as 0.5% NBSK to the system results in a flow pattern change. Many small bubbles are still present, but large bubbles periodically develop near the air injection position and rise through the system. Large bubbles are defined in this study as those that may be influenced by the confining walls. Clift et al. (1978) state that bubbles with an equivalent

diameter d rising through a cylindrical column of diameter D will be unaffected by the cylinder wall if $d \leq 0.6D$. Extending this idea to a bubble rising between two parallel plates, wall effects could be neglected when $d \leq 0.6t$, where t is the distance separating the parallel plates. Approximating the bubble column used in this study as two parallel plates reveals wall effects can be neglected when $d \leq 12$ mm. Therefore, large bubbles correspond to those with an effective diameter greater then 12 mm. The bulk rising air flow oscillates in a serpentine fashion, and the large bubbles follow this pattern. Backmixing is still visually observed when fiber is introduced into the bubble column. Some of the small bubbles become caught in the backmixed flow, but they are eventually entrained in the bulk rising air flow.

The general flow patterns for a 1% NBSK system are revealed in *Fig. 3*. This is a consistency range at which flotation deinking cells typically operate. There are still small bubbles in the system, but the frequency of large bubbles has increased. Some of the large bubbles have an equivalent diameter that is greater than the column thickness of 20 mm and they typically span the entire column depth. The shape of these bubbles deform as they rise through the column due to interaction with the fiber network. In *Fig. 3*, three large bubbles are about to break the surface, which makes the height of the air/fluid interface difficult to identify. Therefore, although there is a considerable amount of gas holdup in this system, the exact value cannot be quantified by the rise in column height. The flow conditions observed here would be considered churn-turbulent where the large bubbles create violent oscillations in the fluid motion (Hewitt 1982). Therefore, fibers promote an early transition from bubbly flow to churn-turbulent flow. This result was also observed by Heindel and Monefeldt (1997, 1998).

Representative FXR images of position 2 for each NBSK consistency addressed in this study are shown in *Fig. 4*. The flexible air hose is visible on the left-hand side of each 20 cm ×

20 cm image. As the fiber consistency increases, the number of small bubbles decreases and the number (and size) of large bubbles increases. This result is clearly evident when the bubble size distribution is determined from multiple position 2 radiographs, as shown in *Fig. 5*. Note that the majority of the bubbles in each population are smaller than 12 mm and there are only a few with equivalent bubble diameters greater than 20 mm, corresponding to the column depth. The average bubble size and standard deviation (*Table 1*) increases with increasing NBSK consistency, but this is primarily the result of the increase in the few number of large bubbles as consistency increases. Although the total number of large bubbles is rather small compared to the entire bubble population, it clearly increases with increasing fiber consistency. One very apparent feature of *Fig. 5* is that the bubble size distribution of relatively small bubbles has a similar shape for all NBSK consistencies addressed in this study, with a peak in the 2-3 mm size range. The main difference is that the magnitude of the peak decreases slightly as the NBSK consistency increases, which is due to the increase in the number of large bubbles. Additionally, the majority of the bubbles remain in the range unaffected by the confining walls (i.e., $d \leq 12$ mm).

The few large bubbles that are recorded by the bubble size measurements increase in number as the NBSK consistency increases. This results in a significant shift in average bubble size and the large increase in standard deviation for each bubble population as the NBSK consistency increases. These large bubbles also serve a very important function by acting as "mobile mixers" in the fiber suspension and maintaining a uniform system throughout the bubble column. This allows the majority of the bubbles to remain relatively small and free to move throughout the system. In terms of flotation deinking cells, the small bubbles would capture ink particles, and the large bubbles would keep the suspension well mixed and prevent fiber network formation. This type of bubble size distribution was not observed in the bubble size

measurements of Heindel (1999) because the air flow rate in that study was much lower than that used here.

The cumulative number density for the various NBSK consistencies is shown in *Fig. 6*. All curves display the same general form and asymptote to a constant cumulative number density when the equivalent bubble diameter is less than 12 mm. The few remaining bubbles in the population comprise the large bubbles with equivalent bubble diameters greater than 12 mm, and for the conditions of this study, can be as large as 44 mm. This figure again shows that the number of large bubbles increases with increasing NBSK consistency.

The similarity in the cumulative number density distributions suggests that it may be possible to characterize the bubble size distributions with a particular type of known distribution. Three such distributions are shown in *Fig. 7* for each NBSK consistency. Since the bubble size is defined only for $d > 0$, the cumulative normal distribution is given by

$$\mathrm{Cum_N} = \int_0^x \frac{1}{\sigma\sqrt{2\pi}} \exp\left[-\frac{1}{2}\left(\frac{y-\mu}{\sigma}\right)^2\right] dy \qquad [1]$$

where y is a dummy variable and x is the parameter of interest (i.e., the bubble diameter), and μ and σ are the mean and standard deviation of the bubble population. The cumulative lognormal distribution is given by

$$\mathrm{Cum_{LN}} = \int_0^x \frac{1}{y\sigma_{LN}\sqrt{2\pi}} \exp\left[-\frac{1}{2}\left(\frac{\ln(y)-\mu_{LN}}{\sigma_{LN}}\right)^2\right] dy \qquad [2]$$

where μ_{LN} and σ_{LN} are the mean and standard deviation of the natural logarithm of the bubble diameters. These values are not equivalent to μ and σ, but can be related by (Ayyub, McCuen 1997)

$$\mu_{LN} = \ln(\mu) - \frac{1}{2}\sigma_{LN}^2 \quad [3]$$

$$\sigma_{LN}^2 = \ln\left[1 + \left(\frac{\sigma}{\mu}\right)^2\right] \quad [4]$$

The cumulative gamma distribution is given by

$$Cum_G = \int_0^x \frac{1}{\beta^\alpha \Gamma(\alpha)} y^{\alpha-1} e^{-y/\beta} dy \quad [5]$$

where $\Gamma(\alpha)$ is the gamma function and α and β are parameters that describe it and are related to μ and σ by (Devore 1982)

$$\mu = \alpha\beta \quad [6]$$

$$\sigma^2 = \alpha\beta^2 \quad [7]$$

For the air/water data, the normal distribution is adequate for describing the bubble size distribution, but the lognormal and gamma distributions follow the experimental data much better. When these three distributions are used to characterize the bubble size distribution in a 0.5% NBSK suspension, the lognormal distribution does a better job at following the experimental data, but it is still not very good. The discrepancy between the data and the various distributions becomes even larger as the NBSK consistency increases and is due to the increased presence of the large bubbles as consistency increases.

By neglecting the small number of bubbles in each bubble population that are influenced by the confining walls ($d > 12$ mm), the cumulative number densities for those bubbles with $d \leq 12$ mm are shown in *Fig. 8*. Normal, lognormal, and gamma distributions are also shown for each NBSK consistency. The specific parameters used to generate these distributions are shown in *Table 2*. For the air/water system, each distribution provides adequate representation of the experimental data, with the normal distribution deviating from the data the most. As the NBSK

consistency increases, the normal distribution fails to follow the experimental data. The gamma distribution also begins to deviate from the experimental data as the NBSK consistency increases. This is particularly apparent at 1.5% consistency. The data for all consistencies are best predicted by the lognormal distribution with the associated parameters given in *Table 2*.

As shown in *Table 2*, the mean (μ_{LN}) and standard deviation (σ_{LN}) of the natural logarithms of the bubble size, with $d \leq 12$ mm, are similar for all NBSK consistencies addressed in this study. Combining all $d \leq 12$ mm data yields average values of $\mu_{LN,ave} = 1.0$ and $\sigma_{LN,ave} = 0.45$. The experimental cumulative number densities for $d \leq 12$ mm and Eq. [2] evaluated at $\mu_{LN,ave}$ and $\sigma_{LN,ave}$ are shown in *Fig. 9*. This distribution does a good job at characterizing the bubble size distribution for all conditions of this study. The data deviate from the lognormal distribution only after the 70th percentile is reached.

IMPLICATIONS TO BUBBLE SIZE CONTROL IN FIBER SUSPENSIONS

As shown in *Fig. 6*, the cumulative number densities of the bubble size distribution are similar for all NBSK consistencies addressed in this study. The minor differences are the result of the few large bubbles that increase in frequency as the NBSK consistency increases. By focusing only on those bubbles with $d \leq 12$ mm, *Fig. 9* shows that the cumulative number density of the bubble population can be characterized by the lognormal distribution (Eq. [2]). Therefore, for a well-mixed system, the presence of fibers has only a minor influence on bubble size of *small* bubbles. However, increasing the fiber consistency increases the number and size of large bubbles (i.e., $d > 12$ mm). These large bubbles act as "mobile mixers" and create churn-turbulent flow conditions, which minimizes floc formation and maintains uniform conditions throughout the system. This was not concluded during an earlier study (Heindel 1999) because in

that study, the air flow rate was not high enough to maintain a well-mixed system, which resulted in fiber network formation.

Although the large bubbles are beneficial from a mixing point of view, the reduced surface area for a given total gas volume is detrimental to any heat or mass transfer operation. A mechanical agitator could perform the same function as the large bubbles and keep the system well-mixed. This would allow all the gas that is injected into a fiber suspension to be utilized for its desired purpose, such as bleaching, heating, or contaminant removal. Additionally, a lower gas flow rate would be required to yield the same results due to the more effective use of the gas.

CONCLUSIONS

Flash x-ray radiography was used to record bubble size distributions in northern bleached softwood kraft pulp suspensions at consistencies as high as 1.5%. The gas flow regime changed from bubbly to churn-turbulent as the NBSK consistency increased. Differences in the cumulative number density of the bubble size distribution for all consistencies were attributed to the few large bubbles that increased in frequency as the consistency increased. Focusing on bubbles unaffected by wall effects ($d \leq 12$ mm), the cumulative number density of the bubble distribution was characterized by a lognormal distribution with $\mu_{LN,ave} = 1.0$ and $\sigma_{LN,ave} = 0.45$ for all fiber consistencies addressed in this study.

ACKNOWLEDGMENT

The work described in this paper was funded by the Member Companies of the Institute of Paper Science and Technology. Their continued support is gratefully acknowledged.

REFERENCES

Ajersch, M., Pelton, R., Towers, M. and Loewen, S. (1992): The Characterization of Dispersed Air in Two Newsprint Paper Machines, J. Pulp Paper Sci., *18*:4, J121.

Ayyub, B.M. and McCuen, R.H. (1997): "Probability, Statistics, & Reliability for Engineers". CRC Press, Boca Raton, Florida.

Clift, R., Grace, J.R. and Weber, M.E. (1978): "Bubble, Drops, and Particles". Academic Press, New York.

Devore, J.L. (1982): "Probability and Statistics for Engineers and the Sciences". Brooks/Cole Publishing Company, Monterey, CA.

Heindel, T.J. (1999): Bubble Size Measurements in a Fiber Suspension, J. Pulp Paper Sci., *25*:3, .

Heindel, T.J. and Monefeldt, J.L. (1997): Flash X-ray Radiography for Visualizing Gas Flows in Opaque Liquid/Fiber Suspensions, 6th International Symposium on Gas-Liquid Two-Phase Flows, Vancouver, BC, ASME Press.

Heindel, T.J. and Monefeldt, J.L. (1998): Observations of the Bubble Dynamics in a Pulp Suspension Using Flash X-ray Radiography, Tappi J., *81*:11, 149.

Hetsroni, G., Ed. (1982): Handbook of Multiphase Systems, Hemisphere Publishing Corp., New York.

Hewitt, G.F. (1982): Flow Regimes, In "Handbook of Multiphase Systems", G. Hetsroni, Ed., New York, Hemisphere Publishing Corp., Chapter 2.1.

Hunold, M., Krauthauf, T., Müller, J. and Putz, H.-J. (1997): Effect of Air Volume and Air Bubble Size Distribution on Flotation in Injector Aerated Deinking Cells, J. Pulp Paper Sci., *23:*12, J555.

Julien Saint Amand, F. (1997): Hydrodynamics of Flotation: Experimental Studies and Theoretical Analysis, In "1997 TAPPI Recycling Symposium", Atlanta, GA, TAPPI Press, 219.

Kerekes, R.J., Soszynski, R.M. and Tam Doo, P.A. (1985): The Flocculation of Pulp Fibres, In "Papermaking Raw Materials", V. Punton, Ed., London, Mechanical Engineering Publications Limited, 265.

Lindsay, J.D., Ghiaasiaan, S.M. and Abdel-Khalik, S.I. (1995): Macroscopic Flow Structure in a Bubbling Paper Pulp-Water Slurry, Ind. Eng. Chem. Res., *34*, 3342.

Pelton, R. and Piette, R. (1992): Air Bubble Holdup in Quiescent Wood Pulp Suspensions, The Can. J. Chem. Eng., *70*, 660.

Saxena, S.C., Patel, D., Smith, D.N. and Ruether, J.A. (1988): An Assessment of Experimental Techniques for the Measurement of Bubble Size in a Bubble Slurry Reactor as Applied to Indirect Coal Liquefaction, Chem. Eng. Commun., *63*, 87.

Schulz, T.H. and Heindel, T.J. (1998): A Study of Gas Holdup in a Cocurrent Air/Water/Fiber System, In "1998 TAPPI Engineering Conference", Atlanta, GA, TAPPI Press, 957.

TAPPI (1994): T 205 om-88 - Forming Handsheets for Physical Tests of Pulp, TAPPI Test Methods 1994-1995, Atlanta, TAPPI Press.

TAPPI (1996): T 413 om-93 - Ash in Wood, Pulp, Paper, and Paperboard: Combustion at 900°C, TAPPI Test Methods 1996-1997, Atlanta, TAPPI Press.

Walmsley, M.R.W. (1992): Air Bubble Motion in Wood Pulp Fibre Suspension, In "APPITA 1992 Proceedings", 509.

Zhu, J.Y. (1996): Laser Doppler Velocimetry for Flow Measurements in Pulp and Paper Research, 1996 Engineering Conference, Chicago, TAPPI Press, 3.

Table 1. Average and standard deviations of the recorded bubble populations.

NBSK Consistency (%)	Average Equivalent Bubble Diameter (mm)	Standard Deviation (mm)
0	3.0	1.2
0.5	3.5	3.6
1	4.2	5.8
1.5	6.3	9.3

Table 2. Parameters used to characterize the bubble distributions for $d \leq 12$ mm.

NBSK Consistency (%)	Normal Distribution		Lognormal Distribution		Gamma Distribution	
	μ (mm)	σ (mm)	μ_{LN} (-)	σ_{LN} (-)	α (-)	β (mm)
0	3.0	1.2	1.0	0.39	6.0	0.51
0.5	3.0	1.2	1.0	0.38	6.5	0.46
1	3.1	1.6	1.0	0.49	3.6	0.84
1.5	3.3	1.9	1.0	0.53	3.1	1.1

LIST OF FIGURES

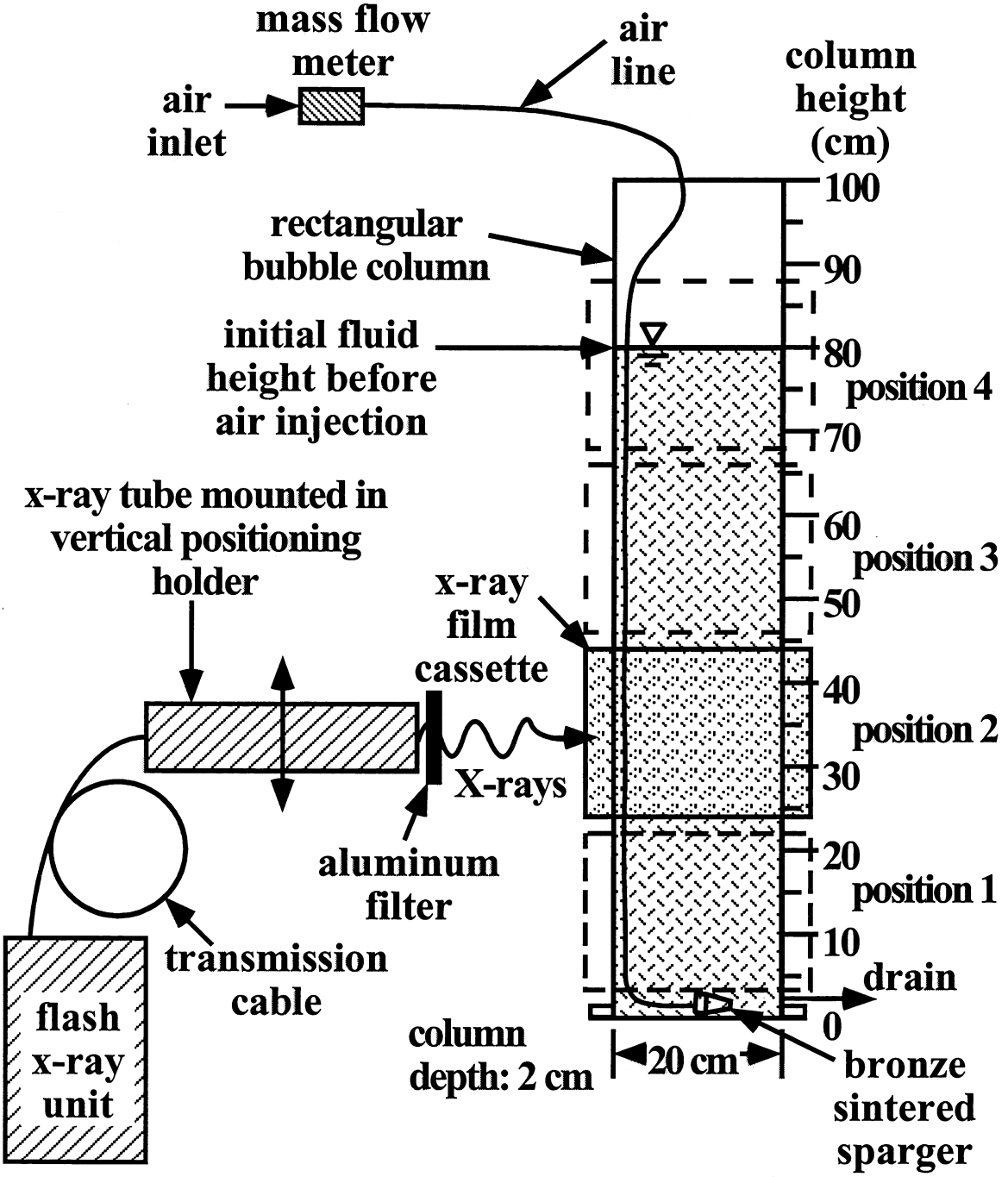
mass flow meter
air inlet
air line
column height (cm)
100
90
80
70
60
50
40
30
20
10
0
rectangular bubble column
initial fluid height before air injection
position 4
position 3
position 2
position 1
x-ray tube mounted in vertical positioning holder
x-ray film cassette
X-rays
aluminum filter
transmission cable
flash x-ray unit
drain
column depth: 2 cm
20 cm
bronze sintered sparger

Figure 1

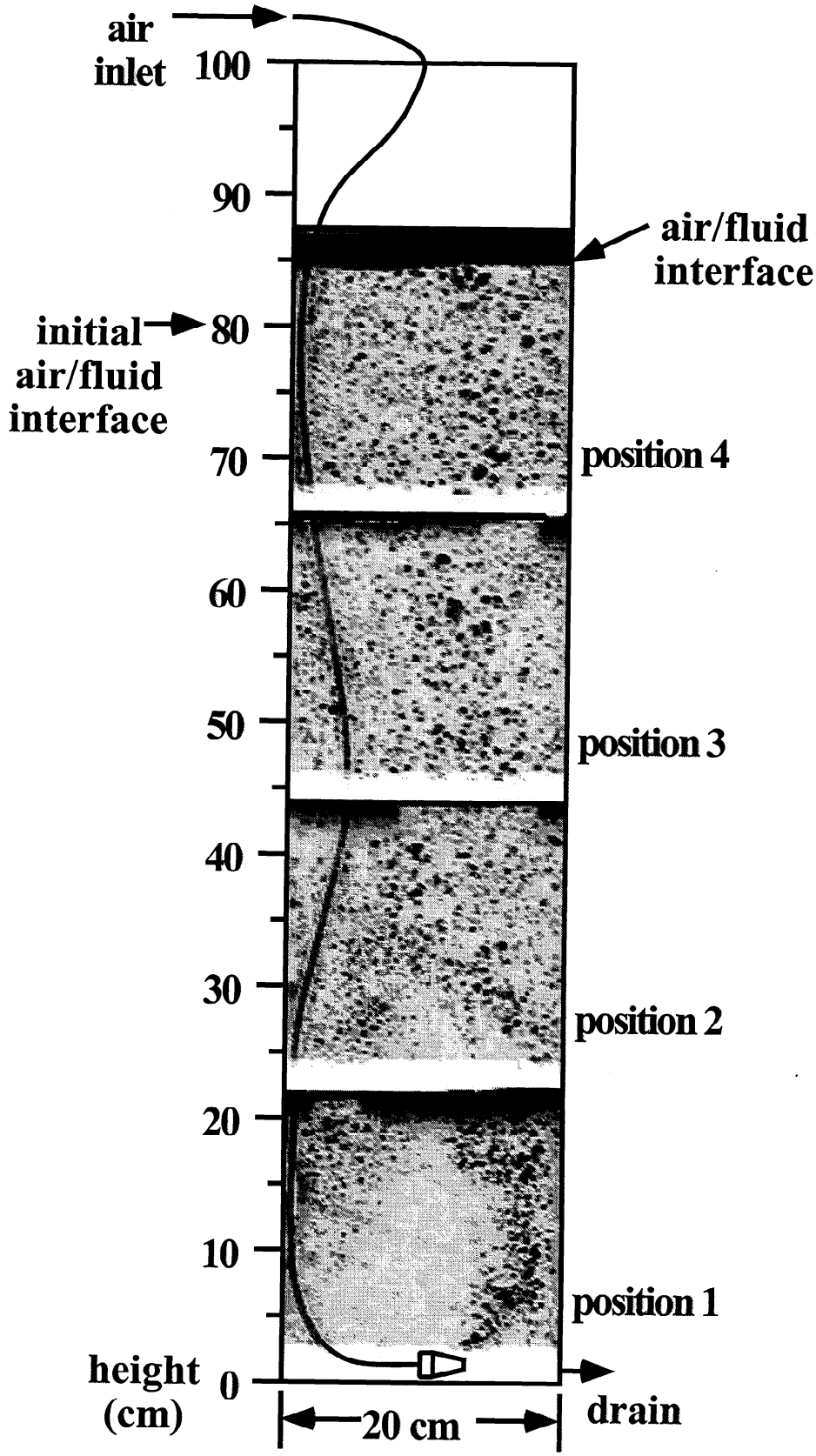
air
inlet
100
90
air/fluid
interface
initial
air/fluid
interface
80
70
position 4
60
50
position 3
40
30
position 2
20
10
position 1
height
(cm)
0
20 cm
drain

Figure 2

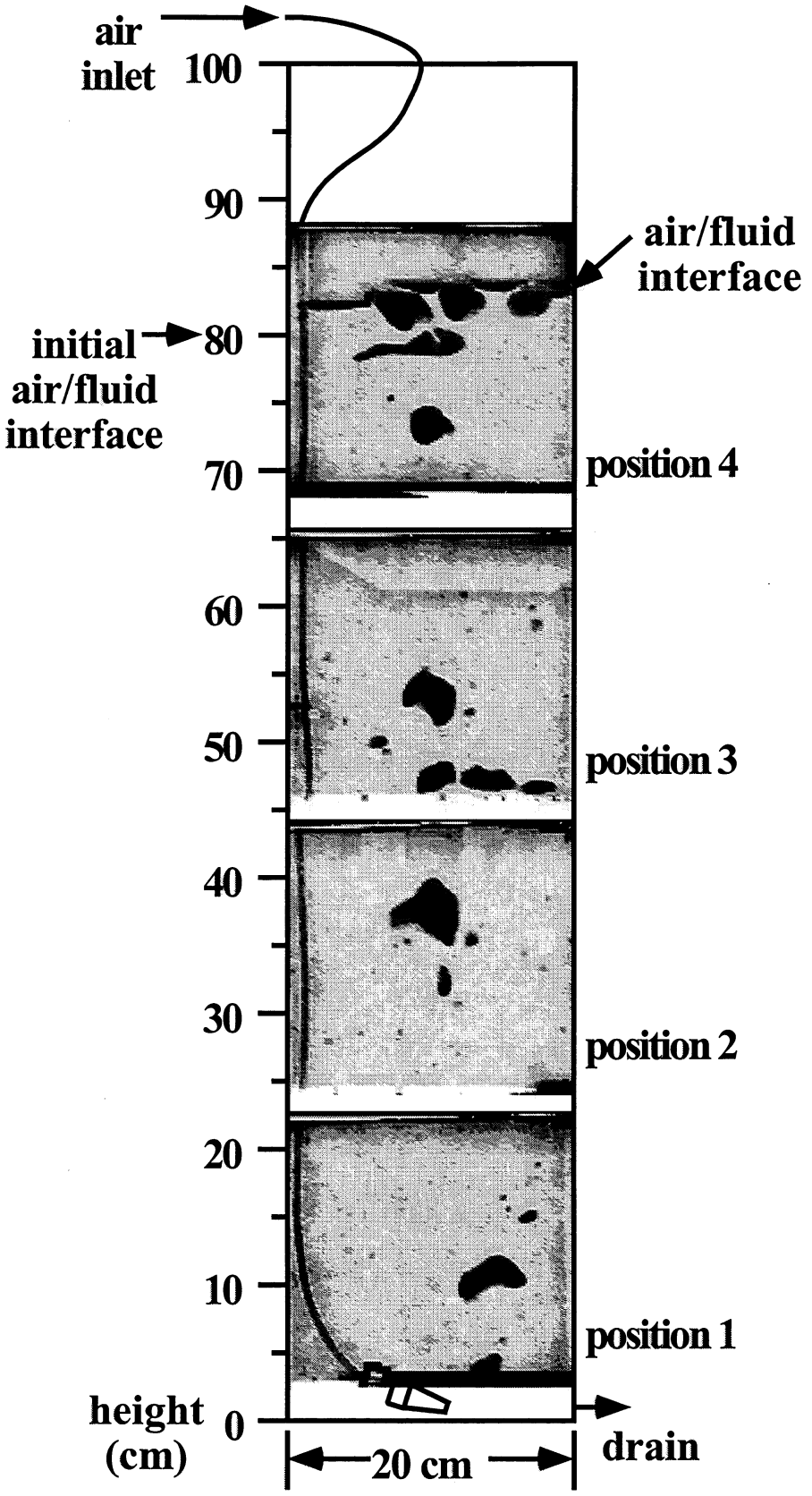
air
inlet
100
90
air/fluid
interface
initial
air/fluid
interface
80
70
position 4
60
50
position 3
40
30
position 2
20
10
position 1
height
(cm)
0
20 cm
drain

Figure 3

(a) air/water system

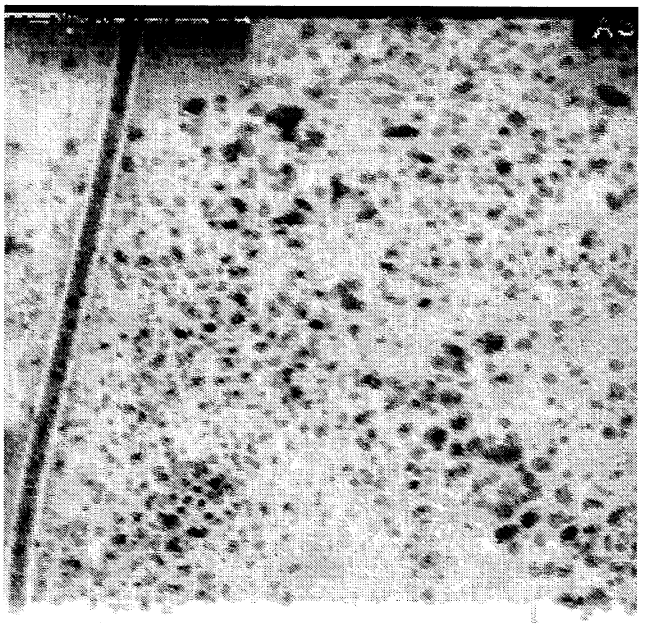

(b) air/water/0.5% NBSK system

(c) air/water/1% NBSK system

(d) air/water/1.5% NBSK system

Figure 4

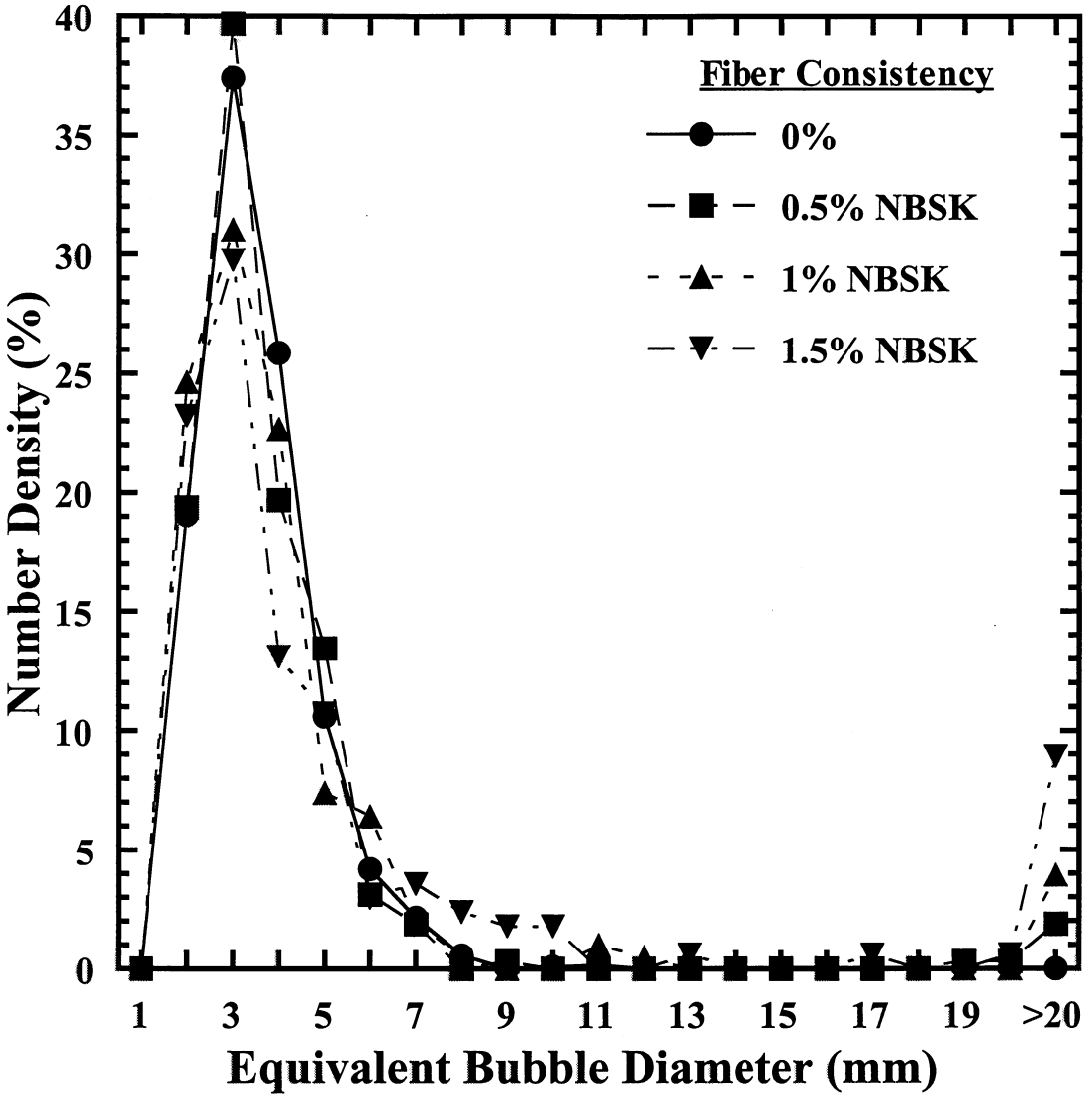
Fiber Consistency
0%
0.5% NBSK
1% NBSK
1.5% NBSK
Number Density (%)
0
5
10
15
20
25
30
35
40
1
3
5
7
9
11
13
15
17
19
>20
Equivalent Bubble Diameter (mm)

Figure 5

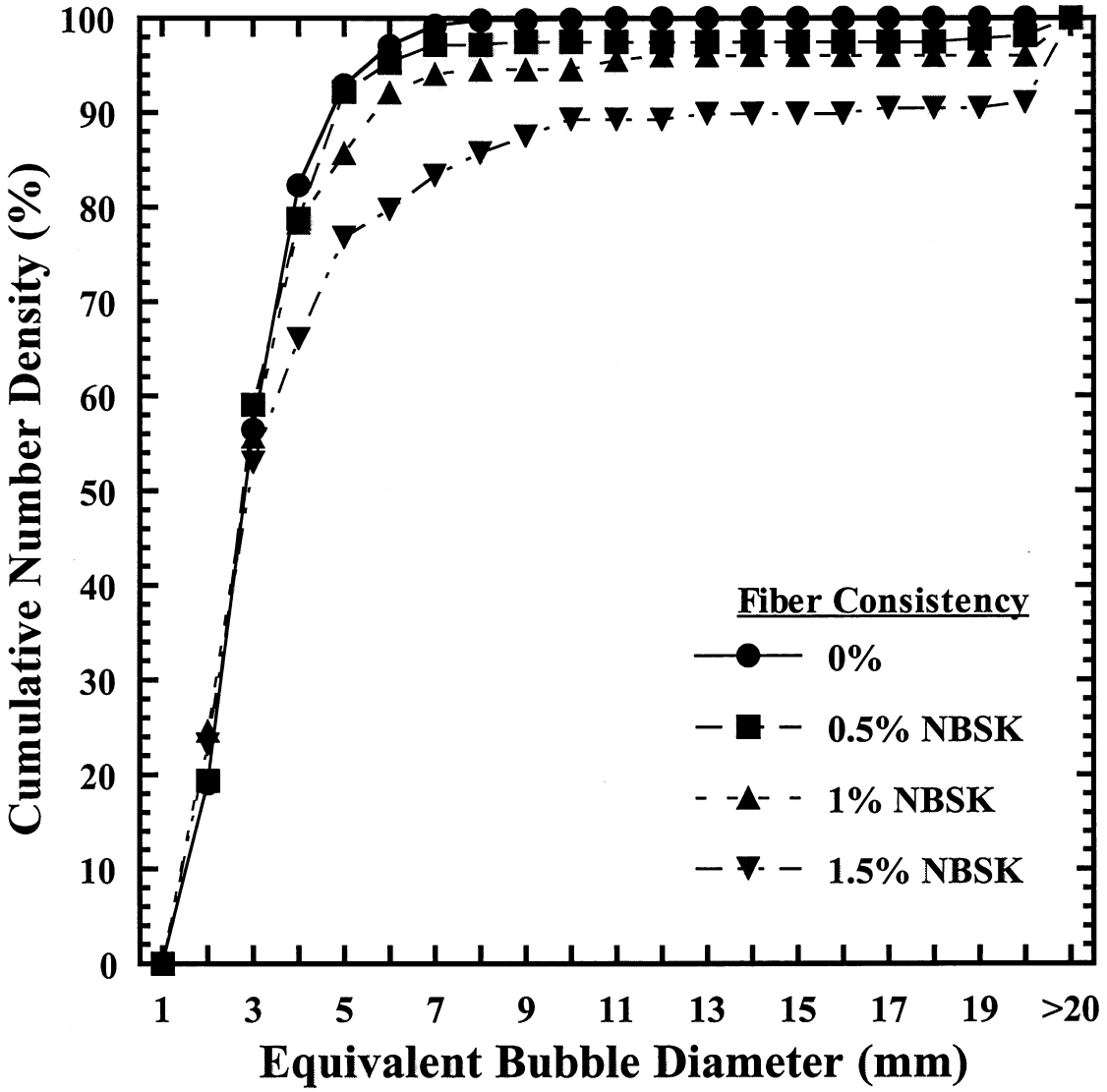
Cumulative Number Density (%)
100
90
80
70
60
50
40
30
20
10
0
1
3
5
7
9
11
13
15
17
19
>20
Equivalent Bubble Diameter (mm)
Fiber Consistency
0%
0.5% NBSK
1% NBSK
1.5% NBSK

Figure 6

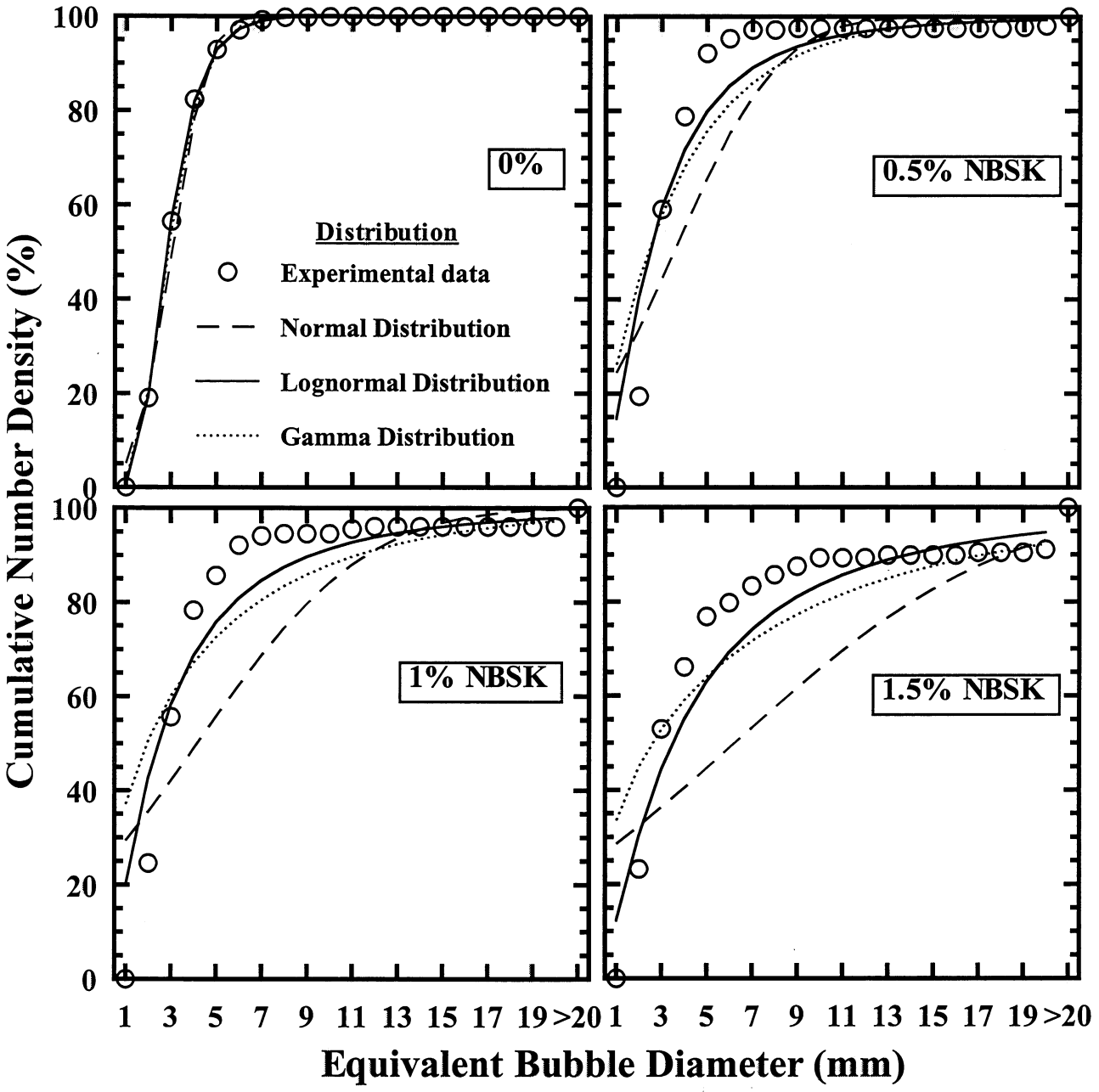
Cumulative Number Density (%)
Equivalent Bubble Diameter (mm)
0%
0.5% NBSK
1% NBSK
1.5% NBSK
Distribution
Experimental data
Normal Distribution
Lognormal Distribution
Gamma Distribution
0
20
40
60
80
100
1 3 5 7 9 11 13 15 17 19 >20

Figure 7

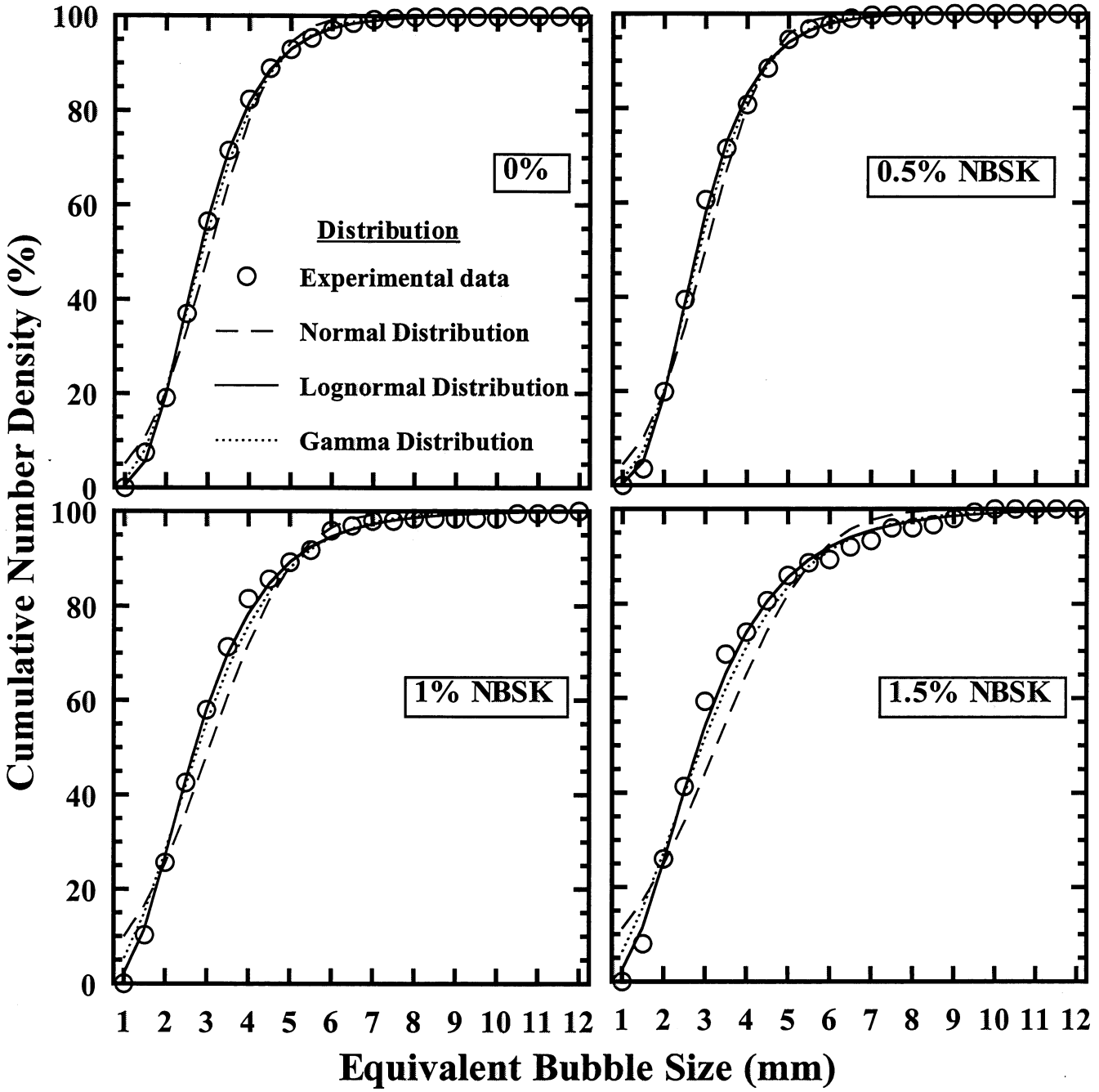
Cumulative Number Density (%)
Equivalent Bubble Size (mm)
0%
0.5% NBSK
1% NBSK
1.5% NBSK
Distribution
Experimental data
Normal Distribution
Lognormal Distribution
Gamma Distribution

Figure 8

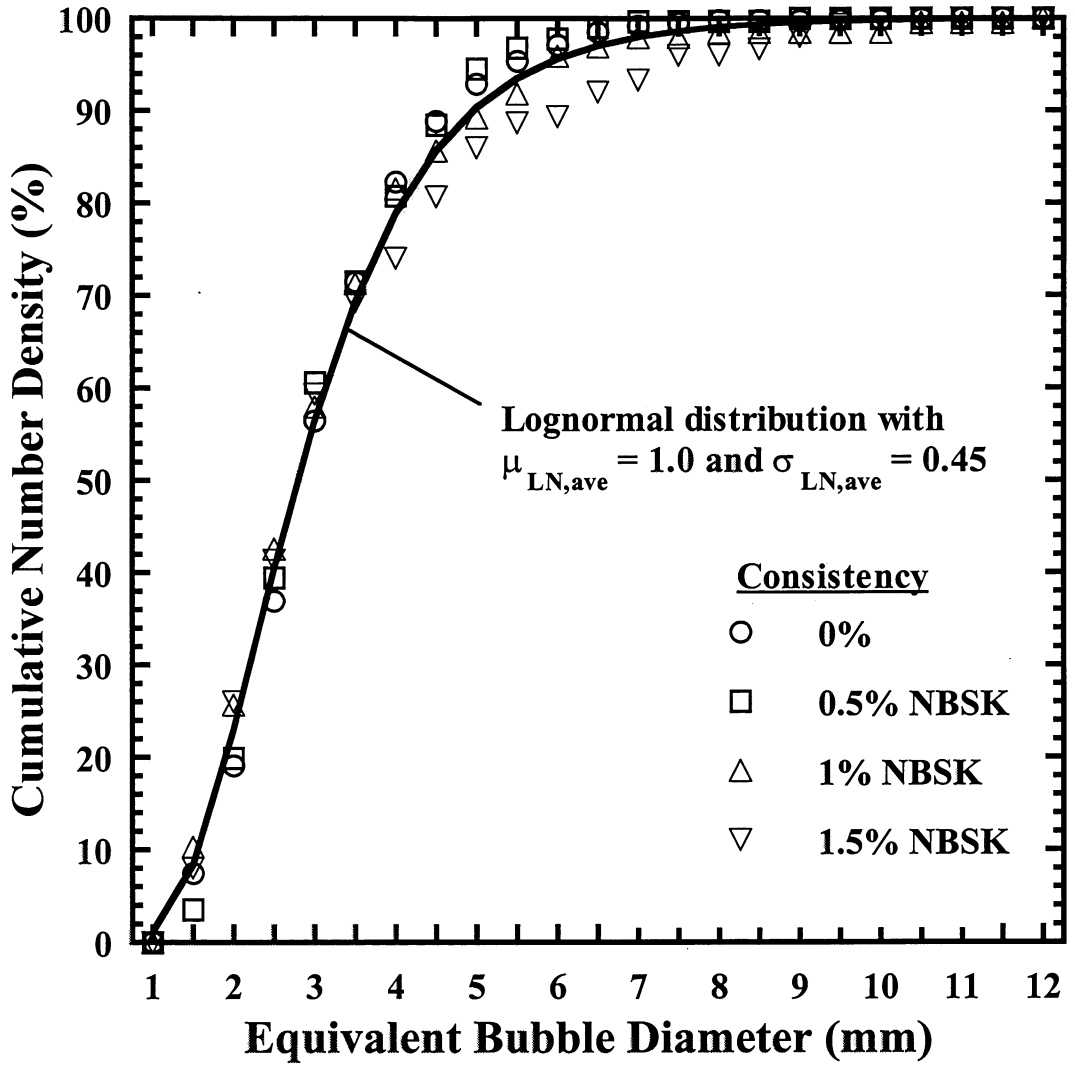
Cumulative Number Density (%)
100
90
80
70
60
50
40
30
20
10
0
1
2
3
4
5
6
7
8
9
10
11
12
Equivalent Bubble Diameter (mm)
Lognormal distribution with
μ LN,ave = 1.0 and σ LN,ave = 0.45
Consistency
0%
0.5% NBSK
1% NBSK
1.5% NBSK

Figure 9